Research Article

ADVANCED PHOTONICS

# High *Q*-factor controllable phononic modes in hybrid phononic–dielectric structures

Bo Qiang,[a,b] Alexander M. Dubrovkin,[a] Harish N. S. Krishnamoorthy,[a] Qian Wang,[c] Cesare Soci,[a] Ying Zhang,[d] Jinghua Teng,[c] and Qi Jie Wang[a,b,*]

[a]Nanyang Technological University, Centre for Disruptive Photonic Technologies, The Photonic Institute, School of Physical and Mathematical Sciences, Singapore

[b]Nanyang Technological University, Centre for OptoElectronics and Biophotonics, School of Electrical and Electronic Engineering, Singapore

[c]Agency for Science, Technology and Research, Institute of Materials Research and Engineering, Singapore

[d]Agency for Science, Technology and Research, Institute of Manufacturing Technology, Singapore

**Abstract.** Phonon polariton resonances in the mid-infrared spectral range demonstrate properties superior to noble metal-based plasmonics, owing to smaller dissipative loss and better field confinement. However, a conventional way to excite the localized phonon resonance involves ion etching, which reduces the attainable quality factors (*Q*-factors) of the resonators. We show that by introducing a deep subwavelength layer of dielectric gratings on a phononic substrate, localized dipolar resonance and higher order modes with high *Q*-factors 96 and 195, respectively, can be excited. We further demonstrate, via experiments and simulations, that the resonant wavelength and field confinement can be controlled by coupling the localized hybrid mode with propagating surface phonon-polaritons. We also observed for the first time the coupling between a localized dipolar mode and a propagating higher-order surface phonon-polariton mode. The results will be useful in designing on-chip, low-loss, and highly integrated phononic devices in the infrared spectral domain.

Keywords: hybrid resonance; high *Q*-factor; phonon resonance; mode splitting.

Received Jan. 29, 2019; accepted for publication Apr. 1, 2019; published online Apr. 23, 2019.



[DOI: 10.1117/1.AP.1.2.026001]

## 1 Introduction

Squeezing photon energy into a deep subwavelength scale opens the path to strong light–matter interactions and has been extensively studied in plasmonics. Numerous applications have been demonstrated using noble metals and plasmonic graphene, which include waveguiding,[1–3] refractive index sensing,[4–6] perfect absorption,[5,7,8] and Purcell factor enhancement,[9,10] to name but a few. However, in the mid-infrared (mid-IR) spectral range, plasmonic materials suffer from either lack of confinement of the plasmon wave (in the case of noble metals) or high optical loss (in the case of graphene), which limit their practical applications. Recent advances in mid-IR phononic technologies provide an effective approach to address these challenges by using polar crystals as an alternative low-loss platform for highly integrated photonics. Such materials enable extremely confined phonon polaritons that exhibit lifetimes one order higher than almost all plasmonic counterparts.

Deep subwavelength confinement, high quality factor (*Q*-factor) resonance and, therefore, high Purcell enhancement have been demonstrated using silicon carbide (SiC),[11–15] hexagonal boron nitride (hBN),[16–18] and molybdenum trioxide ($\alpha$-$MoO_3$).[19,20] Moreover, introducing an ultrathin dielectric layer on top of the phononic substrate can further boost the confinement of the propagating surface wave more than $10^2$ times.[21,22]

To achieve localized phonon resonance, however, all current technologies involve reactive ion etching of the phononic material, which inevitably causes damage to the crystal lattice and absorption of foreign ions in the structure surfaces.[23] These negative effects damp the resonance and reduce achievable *Q*-factors by several times.[12] Although the negative effects could be partially alleviated by postprocessing, alternative

*Address all correspondence to Qi Jie Wang, E-mail: qjwang@ntu.edu.sg

methodologies to excite phonon resonance without damaging the crystal lattice are highly desired. In this work, we demonstrate localized hybrid phononic modes with $Q$-factors as high as 195 by facile lift-off fabrication of ultrathin dielectric structures on SiC substrate, with a thickness more than $10^2$ times smaller than the device operation wavelength (e.g., 70-nm-thick germanium). The achieved $Q$-factor surpasses the theoretical limit of the $Q$-factor of silver nanoparticle and the experimental $Q$-factor of SiC pillars.[12] We further demonstrate that both the field confinement and the resonant wavelength of the phononic modes can be effectively tuned by controlling the coupling between localized hybrid modes with the propagating surface phonon polaritons (SPhPs), which suggests an additional degree of freedom to manipulate the electromagnetic response at mid-IR frequencies.

## 2 Results and Discussion

Figure 1(a) shows a scanning electron microscopy (SEM) image of the fabricated germanium grating on 6H-SiC substrate. The grating is fabricated by standard electron beam lithography process, followed by thermal evaporation of 70-nm undoped germanium and lift-off process. The germanium ribbon and silicon carbide crystal form a hybrid phononic–dielectric cavity similar to the proposed plasmonic–dielectric cavity.[24] Figure 1(b) shows the experimental absorption spectrum of such a hybrid cavity with ribbon width of 2 $\mu$m and period of 4 $\mu$m, normalized by the reflection spectrum of a bare SiC surface. It can be observed that two resonant peaks appear within the spectral range, which are dipolar (~924.4 cm$^{-1}$) and higher order (897.5 cm$^{-1}$) modes in nature. By fitting the spectrum with double-Lorentzian curve, we can extract the detailed information of each mode. The full widths at half maximum of the dipolar mode ($\Gamma_D$) and the higher order mode ($\Gamma_H$) mode are 9.6 and 4.6 cm$^{-1}$, respectively, which provides corresponding $Q$-factors of 96 and 195. The observed $Q$-factor of the dipolar mode is much higher than localized plasmonic resonance $Q$-factors in most of the noble metals and semiconductors,[25,26] graphene nanoresonators,[6] and localized dipolar resonance of SiC nanopillars ($Q \sim 40$ to 50).[12] It is even comparable to the localized monopolar resonance of SiC ($Q \sim 70$ to 130)[12] and dielectric resonators[27] in mid-IR. The $Q$-factor of the higher order mode stays in the range between the reported $Q$-factors of the monopolar mode of SiC nanopillars and hBN nanoresonators ($Q \sim 283$).

It is interesting to note that the higher order mode resonates at the longer wavelength than the dipolar mode. Similar peculiar behavior is observed when there is a topological phase transition causing photonic band inversion.[28] In our case, the underlying mechanism of the observed phenomenon can be explained by the fact that the slope of the dispersion curve ($\omega_{inc} \sim |k_{mode}|$) of the air–Ge–SiC structure is negative. The effective mode wavelength reduces with a longer excitation wavelength, unlike the typical behavior wherein increasing the incident wavelength would redshift the resonant wavelength. Therefore, the higher order mode resonates at low-energy side of the dipolar mode.

When p-polarized light [electromagnetic field vectors are sketched in Fig. 1(a)] is incident on germanium ribbons, only the antisymmetric mode can be excited, and the light energy is localized within 1 $\mu$m from the SiC surface. Figures 1(c) and 1(d) show simulated intensity distribution of light on the grating structure at 924.4 and 897.5 cm$^{-1}$, respectively, which establishes the dipolar and higher order nature of the modes. These data show that the presence of the thin germanium ribbon not only confines light in the lateral direction but also provides extra confinement in the out-of-plane direction ($z$ axis). Figures 1(e) and 1(f) show the percentage of the total light energy that is confined within a distance $d$ from SiC surface for each of the localized mode and for the propagating SPhP mode at the two corresponding resonant wavelengths. It can be clearly seen that both the modes demonstrate better out-of-plane confinement than that from a trivial propagating surface phonon polariton. Quantitatively, 80% of the light energy is

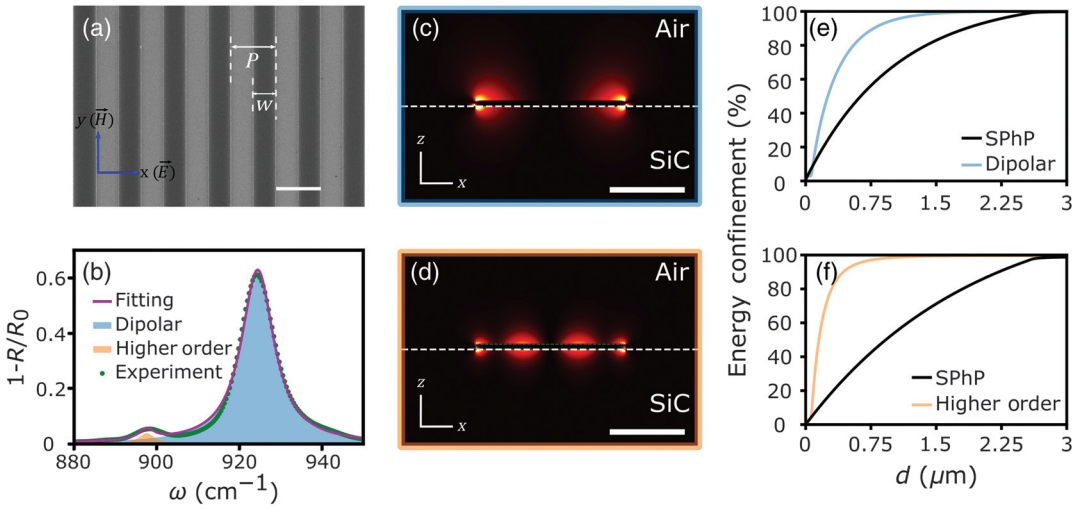


**Fig. 1** Localized hybrid phonon resonance of Ge grating on SiC. (a) SEM image of the grating ($w = 2$ $\mu$m and $P = 4$ $\mu$m). Scale bar equals 4 $\mu$m. (b) Measured absorption spectrum of gratings in (a) and its double-Lorentzian fittings. Simulated intensity distribution of the (c) dipolar and (d) higher order mode. White dashed lines indicate the SiC–air interface. Scale bar equals 4 $\mu$m. (e) and (f) Percentage of total energy localized within a distance $d$ above the SiC surface in the total energy above the SiC surface.

concentrated within 550 nm from the SiC surface when the grating is in dipolar resonance, whereas the SPhP mode at 924.4 $cm^{-1}$ extends more than twice into air (1.4 $\mu$m). The enhancement in the confinement is even more pronounced for the higher order mode, and as a result, the region of 80% energy localization squeezes from 1.84 $\mu$m to 300 nm [Fig. 1(f)]. Such highly confined states of mid-IR energy combined with high resonance *Q*-factors would boost light–matter interactions and may find applications in many areas, such as chemical sensing and thermal emission, bringing pathway to facile fabrication of mid-IR devices.

Furthermore, the interaction of localized and propagating modes can provide peculiar optical phenomena enriching physics of polaritonic systems. This aspect has revealed a plethora of exotic phenomena in plasmonic systems in the past[29–32] but remains rarely studied in phononics.[33] In our system, germanium ribbons may act as building blocks for hybrid resonators and can also collectively form a coupling grating to launch the surface waves on silicon carbide. Propagating SPhPs are excited when the grating period satisfies phase-matching conditions to compensate momentum mismatch between free space photons and the polaritonic wave:

$$\frac{2m\pi}{\Lambda} + k_0 \sin\theta = k_{\mathrm{SPhP}} = k_0\sqrt{\frac{\varepsilon_{\mathrm{SiC}}}{\varepsilon_{\mathrm{SiC}}+1}}, \quad m = \pm 1, \pm 2, \ldots,$$

where $\Lambda$, $\theta$, and $\varepsilon$ denote the grating period, incident angle, and permittivity of SiC, respectively; $k_0$ and $k_{\mathrm{SPhP}}$ are the wavenumber for the light in free space and the complex wavenumber of SPhP existing at the interface between SiC and air, respectively.

Figure 2(b) shows the simulated normalized absorption spectra of germanium gratings on SiC when the grating width is kept constant (2 $\mu$m) but the period is varied. The yellow, magenta, and green dashed lines in the figure indicate phase-matching conditions of SPhP for $\theta = 15$ deg and $m = -1$, 1, and $-2$, respectively. From the figure, we can see that the higher order mode at 887 $cm^{-1}$ remains almost unchanged for all periods. For the dipolar mode, when the grating periods are close to satisfying the phase-matching condition of SPhP mode, it is gradually split into two modes: a higher energy mode (upper branch) and a lower energy mode (lower branch). Within the given grating width range, both $m = -1$ and $m = 1$ orders are coupled with the dipolar mode and cause the mode to split into three resonances. Similar phenomenon was investigated theoretically where the surface phonon polariton of SiC is coupled with two localized resonances.[34] In this paper, we focus on the analysis of the coupling between the localized dipolar mode and the $m = -1$ and $m = 1$ SPhP modes.

The coupling of two modes can create new states of light that share properties of the localized resonance and the propagating mode. For instance, Fig. 2(d) shows the simulated real part of the out-of-plane component of electric field when the grating period is 4 $\mu$m [green dot in Fig. 2(b)]. The field concentrates tightly around germanium ribbons and the light on SiC surface is almost negligible. For the intermediate value of the grating period (6 $\mu$m) shown in Fig. 2(e) [purple dot in Fig. 2(b)], the electric field profile is still dominated by the dipolar response but the confinement starts to decrease compared to Fig. 2(d). The dipolar field leaks further into the air and onto the SiC/air interface between two adjacent germanium ribbons.

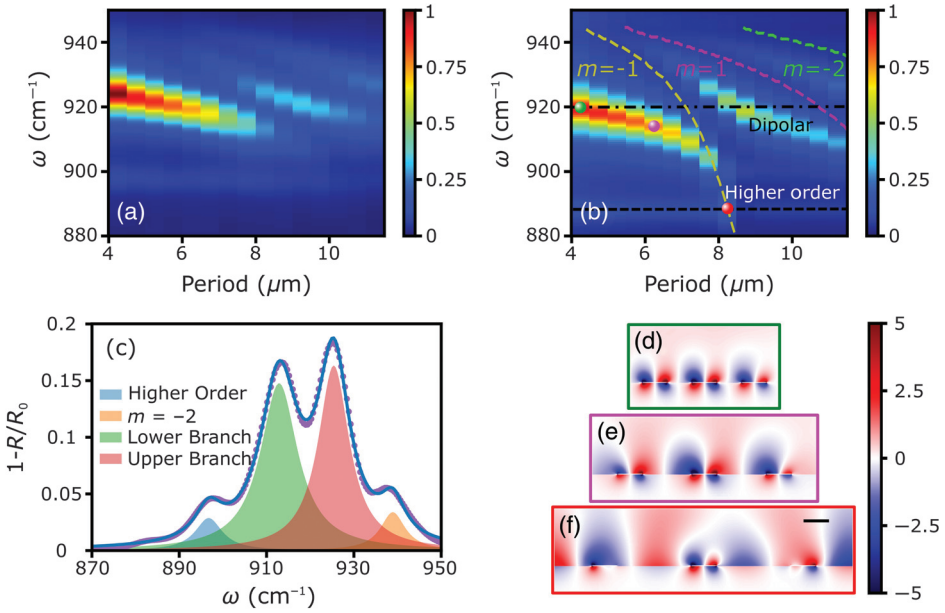


**Fig. 2** Coupling of the propagating SPhP mode with the hybrid phononic–dielectric dipolar mode in Ge gratings with varying period *P* and fixed width ($w = 2$ $\mu$m): (a) experimental normalized absorption and (b) simulated normalized absorption. The yellow, magenta, and green dashed lines indicate phase-matching conditions of SPhP modes with $m = -1$, 1, and –2, respectively. (c) Absorption of the grating when $w = 2$ $\mu$m and $P = 8$ $\mu$m. Shaded areas represent multi-Lorentzian decomposition of the spectrum. Purple dots and blue lines represent experimental data and the fitted spectrum, respectively. (d)–(f) Real parts of the $E_z$ for the green, magenta, and red dots shown in (b), respectively. The scale bar represents 2 $\mu$m.

Finally, Fig. 2(f) shows the field distribution of a 2-$\mu$m Ge grating when the period is 8 $\mu$m at 887 cm$^{-1}$ [red dot in Fig. 2(b)]. The field distribution is no longer the pure dipolar mode as in previous cases, and it partially consists of a surface phonon polariton wave propagating along the grating. The field of the coupled states extends into the air even further than the field shown in Fig. 2(e). This shows how the grating period could be used as a design parameter to tune the near-field energy distributions in the proposed structures.

Figure 2(a) is the experimental plot acquired by measuring reflection spectra when the grating period is tuned from 4 to 11.5 $\mu$m. The absorption spectra are normalized to the reflection of the SiC substrate, and peak absorption is normalized to 1 again to enhance the figure contrast. It captures the main features in the simulations [Fig. 2(b)]. The higher order mode near 897 cm$^{-1}$ remains almost constant for all the gratings. The dipolar and higher order modes are resonant at 924.4 and 897 cm$^{-1}$, respectively, when the grating period is 4 $\mu$m and these values deviate from the simulated resonant frequency by <2%. In addition, the localized dipolar mode couples to the propagating modes of different orders ($m = -1$ and $m = 1$) when the grating period approaches the phase-matching conditions for the SPhP waves. This interaction causes mode splitting and a shift in the resonant frequencies, which qualitatively agree with the simulation. In particular, two hybrid modes are formed when the dipolar mode coupled to the SPhP mode for $m = -1$. When the grating period is increased, the resonant frequency of lower branch gets shifted from 924 to 908 cm$^{-1}$ and the upper branch from 938 to 914 cm$^{-1}$. This shows that the resonant frequency can be tuned by 16 and 24 cm$^{-1}$, respectively, by adjusting the period of the grating. It should be noted that there is a significant difference in the absorption amplitude and the energy separating the two hybrid modes (mode splitting $g$). The simulations show that the maximum absorption can reach about 90% when the grating period is 4 $\mu$m and the mode splitting $g$ is 20 cm$^{-1}$. In the experiment, the absorption is about 60% [Fig. 1(b)] at 4 $\mu$m and the mode splitting is 12.5 cm$^{-1}$ [as shown in Fig. 2(c)] at 8 $\mu$m. These differences could be attributed to a slight deviation of actual materials permittivity from the theoretical model used for calculations. Further efforts to precisely characterize permittivity of germanium and SiC may improve the matching between the calculated and experimental results; however, it would not affect the major conclusions derived in this work.

Lastly, we investigate the case where the grating width is fixed at 1 $\mu$m and period is changed from 4 to 11.5 $\mu$m (Fig. 3). The dipolar resonant wavelength gets further redshifted compared to previous gratings with wider width (Fig. 2), which confirms the negative dispersion nature ($\omega_{\text{inc}} \sim |k_{\text{mode}}|$) of the air–Ge–SiC structure. Both the simulation [Fig. 3(b)] and experiments [Fig. 3(a)] show a smaller resonant absorption peak compared to 2-$\mu$m-width gratings. This could be explained by larger momentum mismatch between the localized resonant mode (characterized by $2\pi/w$) and the free space photons, which reduces the coupling efficiency. The simulation result shows a mode splitting around $P = 8$ $\mu$m when the dipolar mode is coupled to SPhP mode with $m = -1$. The corresponding mode splitting $g$ is 16 cm$^{-1}$, smaller compared to the previous ($w = 2$ $\mu$m) case, which indicates a weaker coupling between the localized mode and SPhPs. In the experimental reflection spectra, the splitting is not clearly observed and the small feature around $P = 8.5$ $\mu$m is typically seen in weak coupling regimes. These observations illustrate that coupling between the localized phonon polariton mode and free space radiation, or between the localized phonon polariton mode and SPhPs can both be controlled by tuning the width of germanium gratings.

## 3 Conclusion

We have shown that, by patterning a thin layer of dielectric structure on a phononic substrate, high $Q$-localized hybrid phononic–dielectric modes can be excited. The properties (resonant wavelength and field confinement) of the excited hybrid mode can be easily manipulated by controlling the coupling of the mode with propagating SPhPs. Tuning either the propagating mode or the localized hybrid mode affects the coupling, and could be controlled by the grating period or by the dielectric ribbon width. Although this work used SiC/Ge as a proof-of-concept demonstration, the configuration can be easily generalized to other material systems. The polar substrate could be selected from common materials used in the semiconductor industry, such as InP, GaAs, $Al_2O_3$, and $SiO_2$, or van der Waals materials such as hBN or $\alpha$-$MoO_3$. Using different materials could extend the operating wavelength range as these materials have distinct reststrahlen bands. The dieletric materials can also be chosen from transition metal dichalcogenide $MoS_2$[22] or phase change material GST.[21] These materials can enable ultrahigh confinement of light energy or reversible switching of the

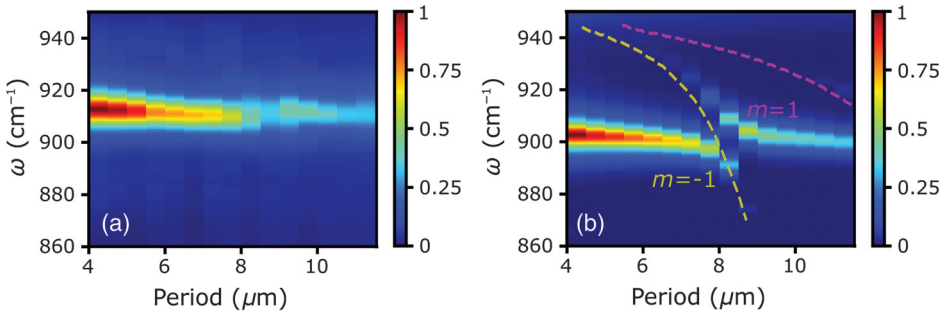


**Fig. 3** Coupling of the propagating SPhP mode with the hybrid phononic–dielectric dipolar mode in Ge gratings with varying period $P$ and fixed width ($w = 1$ $\mu$m): (a) experimental normalized absorption and (b) simulated normalized absorption. The yellow and magenta dashed lines indicate the phase-matching condition of SPhP mode with $m = -1$ and 1, respectively.

phonon mode. Our results are promising for the design and realization of highly integrated, low-loss infrared phononic devices using facile wafer-scale technology.

## Acknowledgments

This work was supported by funding from the Ministry of Education, Singapore (Grant Nos. MOE2016-T2-2-159, MOE2016-T2-1-128, MOE2015-T2-2-007, and MOE Tier 1 RG164/15), the National Research Foundation, Competitive Research Program (No. NRF-CRP18-2017-02), and NSFC (No. 61704082). A.D. acknowledges funding support from the Singapore Ministry of Education Academic Research Funds Tier 3 under Grant No. MOE2016-T3-1-006 (S).

## References

1. J. Christensen et al., "Graphene plasmon waveguiding and hybridization in individual and paired nanoribbons," *ACS Nano* **6**, 431–440 (2011).
2. M. I. Stockman, "Nanofocusing of optical energy in tapered plasmonic waveguides," *Phys. Rev. Lett.* **93**, 137404 (2004).
3. R. F. Oulton et al., "A hybrid plasmonic waveguide for subwavelength confinement and long-range propagation," *Nat. Photonics* **2**, 496–500 (2008).
4. N. Liu et al., "Nanoantenna-enhanced gas sensing in a single tailored nanofocus," *Nat. Mater.* **10**, 631–636 (2011).
5. N. Liu et al., "Infrared perfect absorber and its application as plasmonic sensor," *Nano Lett.* **10**, 2342–2348 (2010).
6. D. Rodrigo et al., "Mid-infrared plasmonic biosensing with graphene," *Science* **349**, 165–168 (2015).
7. Y. Yao et al., "Electrically tunable metasurface perfect absorbers for ultrathin mid-infrared optical modulators," *Nano Lett.* **14**, 6526–6532 (2014).
8. S. Kim et al., "Electronically tunable perfect absorption in graphene," *Nano Lett.* **18**, 971–979 (2018).
9. J. Kern et al., "Nanoantenna-enhanced light-matter interaction in atomically thin $WS_2$," *ACS Photonics* **2**, 1260–1265 (2015).
10. C. Ciracì et al., "Probing the ultimate limits of plasmonic enhancement," *Science* **337**, 1072–1074 (2012).
11. J.-J. Greffet et al., "Coherent emission of light by thermal sources," *Nature* **416**, 61–64 (2002).
12. J. D. Caldwell et al., "Low-loss, extreme subdiffraction photon confinement via silicon carbide localized surface phonon polariton resonators," *Nano Lett.* **13**, 3690–3697 (2013).
13. T. Wang et al., "Optical properties of single infrared resonant circular microcavities for surface phonon polaritons," *Nano Lett.* **13**, 5051–5055 (2013).
14. T. Wang et al., "Phonon-polaritonic bowtie nanoantennas: controlling infrared thermal radiation at the nanoscale," *ACS Photonics* **4**, 1753–1760 (2017).
15. Y. Chen et al., "Spectral tuning of localized surface phonon polariton resonators for low-loss mid-IR applications," *ACS Photonics* **1**, 718–724 (2014).
16. J. D. Caldwell et al., "Sub-diffractional volume-confined polaritons in the natural hyperbolic material hexagonal boron nitride," *Nat. Commun.* **5**, 5221 (2014).
17. A. J. Giles et al., "Imaging of anomalous internal reflections of hyperbolic phonon-polaritons in hexagonal boron nitride," *Nano Lett.* **16**, 3858–3865 (2016).
18. M. Tamagnone et al., "Ultra-confined mid-infrared resonant phonon polaritons in van der Waals nanostructures," *Sci. Adv.* **4**, eaat7189 (2018).
19. Z. Zheng et al., "Highly confined and tunable hyperbolic phonon polaritons in van der Waals semiconducting transition metal oxides," *Adv. Mater.* **30**, 1705318 (2018).
20. W. Ma et al., "In-plane anisotropic and ultra-low-loss polaritons in a natural van der Waals crystal," *Nature* **562**, 557–562 (2018).
21. P. Li et al., "Reversible optical switching of highly confined phonon–polaritons with an ultrathin phase-change material," *Nat. Mater.* **15**, 870–875 (2016).
22. A. M. Dubrovkin et al., "Ultra-confined surface phonon polaritons in molecular layers of van der Waals dielectrics," *Nat. Commun.* **9**, 1762 (2018).
23. N. Ocelic and R. Hillenbrand, "Subwavelength-scale tailoring of surface phonon polaritons by focused ion-beam implantation," *Nat. Mater.* **3**, 606–609 (2004).
24. Y. Yang et al., "Low-loss plasmonic dielectric nanoresonators," *Nano Lett.* **17**, 3238–3245 (2017).
25. L.-W. Chou et al., "Tunable mid-infrared localized surface plasmon resonances in silicon nanowires," *J. Am. Chem. Soc.* **134**, 16155–16158 (2012).
26. G. Dayal et al., "High-*Q* plasmonic infrared absorber for sensing of molecular resonances in hybrid lead halide perovskites," *J. Appl. Phys.* **122**, 073101 (2017).
27. A. Tittl et al., "Imaging-based molecular barcoding with pixelated dielectric metasurfaces," *Science* **360**, 1105–1109 (2018).
28. M. A. Gorlach et al., "Far-field probing of leaky topological states in all-dielectric metasurfaces," *Nat. Commun.* **9**, 909 (2018).
29. W. Ren et al., "Tailoring the coupling between localized and propagating surface plasmons: realizing Fano-like interference and high-performance sensor," *Opt. Express* **21**, 10251 (2013).
30. M. Sarkar et al., "Hybrid plasmonic mode by resonant coupling of localized plasmons to propagating plasmons in a Kretschmann configuration," *ACS Photonics* **2**, 237–245 (2015).
31. S. Balci, E. Karademir, and C. Kocabas, "Strong coupling between localized and propagating plasmon polaritons," *Opt. Lett.* **40**, 3177 (2015).
32. C. V. Hoang et al., "Interplay of hot electrons from localized and propagating plasmons," *Nat. Commun.* **8**, 771 (2017).
33. C. R. Gubbin et al., "Strong and coherent coupling between localized and propagating phonon polaritons," *Phys. Rev. Lett.* **116**, 246402 (2016).
34. C. R. Gubbin, S. A. Maier, and S. De Liberato, "Theoretical investigation of phonon polaritons in SiC micropillar resonators," *Phys. Rev. B* **95**, 35313 (2017).

**Bo Qiang** received his BEng degree from Nanyang Technological University (NTU), Singapore, in 2014, with a major in electrical and electronic engineering. Currently, he is PhD candidate and a project officer in the School of Electrical and Electronic Engineering, NTU. His research interests include metamaterials, metasurfaces, nearfield imaging, and phonon and plasmon resonance in low dimensional materials.

**Qi Jie Wang** received his BE degree in electrical engineering from the University of Science and Technology of China, Hefei, China, in 2001, and his PhD in electrical and electronic engineering from NTU, Singapore, in 2005. His current research interests are to explore theoretically and experimentally nanostructured semiconductor and fiber-based materials, and nanophotonic devices (nanoplasmonics, photonic crystals, and metamaterials) with an emphasis on all aspects of the problem, from design, fabrication, and characterization, to integration at system level.

Biographies of the other authors are not available.